The displacement coefficient method in near-source conditions

Georgios Baltzopoulos, Eugenio Chioccarelli and Iunio Iervolino*,†

Dipartimento di Strutture per l'Ingegneria e l'Architettura, Università degli Studi di Napoli Federico II, Naples, Italy

SUMMARY

The use of nonlinear static procedures for performance-based seismic design (PBSD) and assessment is a well-established practice, which has found its way into modern codes for quite some time. On the other hand, near-source (NS) ground motions are receiving increasing attention, because they can carry seismic demand systematically different and larger than that of the so-called ordinary records. This is due to phenomena such as rupture forward directivity (FD), which can lead to distinct pulses appearing in the velocity time-history of the ground motion. The framework necessary for taking FD into account in probabilistic seismic hazard analysis (PSHA) has recently been established. The objective of the present study is to discuss the extension of nonlinear static procedures, specifically the displacement coefficient method (DCM), with respect to the inelastic demand associated with FD. In this context, a methodology is presented for the implementation of the DCM toward estimating NS seismic demand, by making use of the results of NS-PSHA and a semi-empirical equation for NS-FD inelastic displacement ratio. An illustrative application of the DCM, with explicit inclusion of NS-pulse-like effects, is given for a set of typical plane R/C frames designed under Eurocode provisions. Different scenarios are considered in the application and nonlinear dynamic analysis results are obtained and discussed with respect to the static procedure estimates. Conclusions drawn from the results may help to assess the importance of incorporating NS effects in PBSD. Copyright © 2014 John Wiley & Sons, Ltd.

1. INTRODUCTION

Sites located in proximity to seismic faults are prone to phenomena collectively known as near-source (NS) effects. The most important among these, from a structural engineering perspective, is rupture forward directivity (FD). During fault rupture, shear dislocation may propagate at velocities similar to the shear wave velocity; as a result, there is a probability that, at sites aligned along the direction of rupture propagation, shear wave-fronts generated at different points along the fault arrive at the same time, delivering most of the seismic energy in a single double-sided pulse registered early in the velocity recording. Such impulsive behavior, which is actually the result of constructive interference of horizontally polarized waves, is most prominent in the fault-normal component of ground motion [1]. These pulses have an appreciable effect on spectral pseudo-acceleration (S_a) [2].

Recent advances in probabilistic seismic hazard analysis (PSHA), expressed in terms of rate of exceedance of ground motion intensity measures (IMs), allow FD effects to be accounted for during hazard calculations [3, 4]. On the other hand, inelastic structural response to pulse-like ground

---

*Correspondence to: Iunio Iervolino, Dipartimento di Strutture per l'Ingegneria e l'Architettura, Università degli Studi di Napoli Federico II, via Claudio 21, 80125, Naples, Italy.
†E-mail: iunio.iervolino@unina.it

motions may be systematically different from that to non-impulsive, or *ordinary*, records. Previous investigations have shown that impulsive FD records may exhibit unexpected inelastic displacement demand at periods of elastic vibration equal to some fraction of the pulse period, T_p, or other ground motion parameters (e.g., predominant period) [5–7].

These issues motivate the investigation of FD effects on current structural design procedures. The objective of the present study is to address the importance of extending the applicability of a nonlinear static procedure of structural analysis, namely the displacement coefficient method (DCM), to cases where the structure is found under NS conditions. Recent research results about estimation of elastic and inelastic NS seismic demand are combined in order to develop the methodology.

The remainder of this article is structured so that an introductory presentation of key concepts associated with the DCM is given first. Then, the evaluation of NS elastic and inelastic seismic demand, the former corresponding to seismic hazard analysis, is briefly outlined. At this point, specific NS design scenarios, deemed meaningful for the following investigations, are presented. Subsequently, implementation of the DCM in NS conditions is illustrated by means of example applications. Results are discussed with respect to the case in which FD effects are not explicitly accounted for, and also with respect to the different site-to-source geometric configurations and the source seismicity models considered. Sets of design ground motions representative of some of these NS scenarios are assembled, and nonlinear dynamic analysis results are obtained and discussed against DCM-estimated inelastic demand. Finally, conclusions regarding performance-based seismic design in NS environments are presented.

2. THE DISPLACEMENT COEFFICIENT METHOD

Performance-based seismic design of new structures—or assessment of existing ones—requires that the engineer be able to obtain estimates of structural response well into the inelastic range. Traditional methods based on linear-elastic analysis may be inadequate, whereas fully nonlinear dynamic analysis can present the engineer with a task of daunting effort demand. The development of approximate procedures, based on static nonlinear analysis of structures, thus emerged as a compromise, offering relative simplicity, while still explicitly treading beyond the elastic limit.

The key concept underlying static nonlinear analysis procedures is to represent the structure by a substitute yielding SDOF system and to subsequently use the inelastic spectral response of this system (for given elastic demand at each performance level) as a proxy for the inelastic demand of the original structure. Typically, a *capacity*, or *pushover*, force versus displacement curve is derived starting from a nonlinear model of the structure. This curve is then approximated by a simpler (typically bilinear) relation, which is in turn used to derive the characteristics of the substitute (or equivalent) yielding single degree of freedom (SDOF) system representing the structure. It is well known that this representation has limitations, depending primarily on the structure of interest. The interested reader is referred to [8] for a more thorough discussion.

The transition from elastic demand (e.g., determined by seismic hazard) to inelastic displacement at the SDOF level is generally achieved by employing inelastic response spectra [9]. The required inelastic spectra are traditionally derived via semi-empirical models based on the response of yielding SDOF oscillators subjected to a sample of recorded ground motions. These spectra can be presented in the form of constant strength (C_R) or constant-ductility inelastic displacement ratios.

As far as the DCM in particular is concerned, the conceptual foundations were developed in [10]. It was widely introduced to engineers with its adoption by the publications on seismic rehabilitation by the US Federal Emergency Management Agency (FEMA) [11, 12]. Improvements to the method were subsequently suggested in [13] and are also considered here. The DCM attempts to estimate the inelastic displacement demand of the structure, which corresponds to a reference degree of freedom and is termed the target displacement, δ_t, by applying a succession of modification factors upon the elastic spectral response of the *corresponding* infinite-strength linear SDOF system, Equation (1).

$$\delta_t = C_0 \cdot C_1 \cdot C_2 \cdot C_3 \cdot S_a \cdot \frac{T^2}{4\pi^2} \tag{1}$$

In Equation (1), S_a is chosen to represent elastic demand and forms the basis for design. It is derived from seismic hazard provided as a pseudo-acceleration design spectrum corresponding to the performance level considered. Thus, $S_a \cdot (T^2/4\pi^2)$ represents elastic spectral displacement, $S_{d,e}$, of the corresponding SDOF system having a period of natural vibration equal to T. Coefficients C_0, C_1, C_2, C_3 are intended to transform this elastic SDOF response to inelastic structural response. More specifically, C_0 converts the displacement of the equivalent SDOF system into that of the original multiple DOF (MDOF) structure. C_1 is termed the (constant strength) inelastic displacement ratio and is defined as the peak displacement response $S_{d,inel}$ of an inelastic SDOF system divided by $S_{d,e}$; see also the next section.

C_2 is intended to account for the effect of hysteretic behavior on maximum inelastic displacement, in the case of cyclic stiffness and/or strength degradation. This implies that for the derivation of C_1, non-evolutionary hysteretic relationships are used, as originally envisioned in [10]. An alternative approach can be to evaluate inelastic displacement ratios for degrading SDOF systems directly, as was the case in [14] and also in [15] for NS-FD ground motions. In [5], the effect of cyclic structural degradation on inelastic displacement ratios for pulse-like ground motions was studied but without suggesting any relation applicable for C_2 in NS conditions. Another study, [16], proposed an improved relation for C_2, having also investigated the effect of degradation on the inelastic response to pulse-like NS records. According to [17], implementing *moderate* stiffness degradation during response history analysis (RHA) of several generic frames, led to an average increase of peak roof displacement of the order of 7%, when compared with corresponding analyses with bilinear behavior. While following one of the aforementioned approaches to also incorporate a modified coefficient C_2 in this adaptation of the DCM for NS conditions appears feasible, the added complexity could hinder the objective evaluation of the resulting demand estimates. With this in mind, in the applications presented later on in this paper, exclusively modern code-conforming buildings are considered, exhibiting a beam-sway mechanism at collapse, for which it is assumed that only limited degradation occurs. Therefore, C_2 coefficient is constrained to unity in what follows.

Last, coefficient C_3 was aimed at accounting for increased inelastic displacements in cases where second order (or *P*-Δ) effects become an important factor resulting in negative post-yield stiffness for the equivalent SDOF approximation. It was suggested in [13] that instead of a displacement modification coefficient, an upper limit on strength reduction factor (to follow) should be considered, beyond which dynamic instability is likely to occur. In [18], it is reported that pulse-like ground motions may be more sensitive to phenomena of dynamic instability due to *P*-Δ effects than non-pulse-like ground motions. However, the issue of whether the C_3 coefficient should be maintained, or not, remains outside the scope of the present study and C_3 is also taken as unity hereafter.

3. DISPLACEMENT RATIOS OF ORDINARY AND PULSE-LIKE RECORDS

In [13], it was recommended that inelastic displacement ratio C_1 be estimated from Equation (2), depending on strength reduction factor, R, and a site-subsoil-dependent parameter α (T is the period of vibration).

$$C_1 = C_{R|nopulse} = \begin{cases} 1 + (R - 1)/(0.04 \cdot \alpha) & T < 0.20 \text{ s} \\ 1 + (R - 1)/(\alpha \cdot T^2) & 0.20 \text{ s} \leqslant T < 1.00 \text{ s} \\ 1.00 & T \geqslant 1.00 \text{ s} \end{cases} \qquad (2)$$

The strength reduction factor R appearing in Equation (2), is the reciprocal of SDOF yield strength, F_y, normalized with respect to the maximum elastic force induced by the ground motion on an infinitely elastic SDOF structure, F_e, (Equation (3)).

$$R = F_e/F_y \qquad (3)$$

In fact, inelastic displacement ratios of NS-pulse-like ground motions, systematically differ, both in amplitude and shape, from those obtained for ordinary ground motions, and it was discussed in [5] that C_1, as given by Equation (2), is not explicitly representative of the particular spectral shape associated with impulsive records. Hence, the notation $C_{R|nopulse}$ for C_1, which indicates that Equation (2), is hereafter used when ordinary (non-impulsive) ground motions are considered.

In [6], Equation (4) was proposed for the (constant strength) inelastic displacement ratio, $C_{R|pulse}$, based on a dataset of pulse-like FD ground motions identified as such in previous works [2, 19]. Using nonlinear regression, estimates were obtained for the parameters θ_i $\{i = 1, 2, 3, 4, 5\}$ and are given in Table I. A graphical representation of Equation (4) is provided in Figure 1. The most important feature of this analytical model for $C_{R|pulse}$ is the use of normalized period T/T_p as a predictor variable in order to capture the spectral regions of inelastic response amplification.

$$C_{R|pulse} = \frac{S_{d,inel}}{S_a \cdot \left(T^2/4\pi^2\right)} = 1 + \theta_1 \cdot (T_p/T)^2 \cdot (R - 1) + \theta_2 \cdot (T_p/T) \cdot \exp\left\{\theta_3 \cdot \left[\ln(T/T_p - 0.08)\right]^2\right\}$$
$$+ \theta_4 \cdot (T_p/T) \cdot \exp\left\{\theta_5 \cdot \left[\ln(T/T_p + 0.5 + 0.02 \cdot R)\right]^2\right\} \quad (4)$$

4. NEAR-SOURCE HAZARD, DISAGGREGATION AND INELASTIC DEMAND

Near-source PSHA [3, 4, 20] computes the rate (λ) of exceedance of any IM (spectral pseudo-acceleration at 5% damping ratio is invariably used hereafter) threshold, as the sum of the rates of two independent homogeneous Poisson processes (then mutually exclusive in an infinitesimal time interval), one accounting for ground motions without pulse-like characteristics $\left(\lambda_{S_a,nopulse}\right)$ and one for those with pulses $\left(\lambda_{S_a,pulse}\right)$, as shown in Equation (5).

$$\lambda_{S_a}(s_a) = \lambda_{S_a,nopulse}(s_a) + \lambda_{S_a,pulse}(s_a) \quad (5)$$

The interested reader is referred to the cited studies for details and discussions; here, only the main features of NS-PSHA are recalled to highlight the differences with respect to the classical applications

Table I. Coefficient estimates for Equation (4).

	$R = 2$	$R = 3$	$R = 4$	$R = 5$	$R = 6$	$R = 7$	$R = 8$
θ_1	0.0151	0.0209	0.0211	0.0198	0.0184	0.0170	0.0157
θ_2	−0.146	−0.230	−0.293	−0.343	−0.384	−0.417	−0.445
θ_3	−2.878	−2.360	−2.375	−2.437	−2.444	−2.441	−2.434
θ_4	0.066	0.146	0.193	0.217	0.224	0.232	0.242
θ_5	−47.93	−40.97	−32.70	−27.17	−20.97	−17.21	−15.18
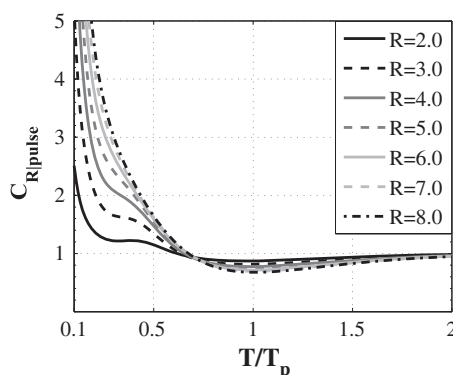
Figure 1. Inelastic displacement ratio of near-source pulse-like ground motions according to [6].

of PSHA: (i) $\lambda_{S_a,pulse}(s_a)$ is implicitly weighted by the probability of pulse, which is provided by semi-empirical models as a function of the site's location relative to rupture [4]; (ii) $\lambda_{S_a,pulse}(s_a)$ accounts for pulse-like features of ground motions via a ground motion prediction equation reflecting the spectral shape of impulsive records [2], and a pulse period distribution conditional on earthquake magnitude [20]; (iii) finally, $\lambda_{S_a,nopulse}(s_a)$ accounts for the non-pulse-like contribution to the hazard and retains the expression of the classical hazard integral, yet is weighted by the complementary to one of the pulse occurrence probability used for $\lambda_{S_a,pulse}(s_a)$.

Once NS-PSHA results are available, disaggregation can be performed [21]. Given, for example, the exceedance (or occurrence) of an IM value of interest, it serves to obtain the probabilities of any of the variables involved in the hazard assessment being causative for such an exceedance (or occurrence). In fact, the probability density function (PDF) of pulse period, $f_{T_P|S_a(T)=s_a,pulse}$, conditional on the occurrence of a given design hazard threshold, $S_a(T)=s_a$, is relevant in the implementation of the DCM in NS conditions, as it is required in order to directly compute the expected value of C_R given the design hazard, according to Equation (6).

$$E[C_R|S_a(T) = s_a, pulse] = \int_{t_p} E[C_R|S_a(T) = s_a, T_P = t_p, pulse] \cdot f_{T_P|S_a(T)=s_a,pulse}(t_p) \cdot dt_p \qquad (6)$$

The conditional expected value, $E[C_R|S_a(T)=s_a, T_P=t_p, pulse]$, corresponds to $C_{R|pulse}$ of Equation (4), once T is fixed, and serves to compute the design inelastic displacement demand, $\delta_{t|pulse}$, in the case of pulse-like ground motions when implementing the DCM. Indeed, if the probability of pulse occurrence, conditional to the design hazard, $P[pulse|S_a(T)=s_a]$, is also obtained from disaggregation, then the inelastic design displacement demand, δ_t^{NS}, may be estimated as in Equation (7). In the equation, which is an application of the *total expectation law*, derived by the *total probability theorem* [22], $\delta_{t|nopulse}$ is the design demand in the case of absence of pulse-like features in the ground motion.

$$\delta_t^{NS} = \delta_{t|pulse} \cdot P[pulse|S_a(T) = s_a] + \delta_{t|nopulse} \cdot (1 - P[pulse|S_a(T) = s_a]) \qquad (7)$$

It is to note that Equation (7), is no different from what is carried out in classical applications of the DCM (and other nonlinear static procedures), which may be interpreted as estimating the expected value of inelastic SDOF demand conditional to elastic design hazard [9]. In the adaptation of the DCM to NS conditions herein, what is simply explicitly accounted for is the additional information about the likelihood of occurrence of an impulsive ground motion and its effect.

5. DESIGN SCENARIOS AND BUILDING MODELS

5.1. Probabilistic hazard with and without pulse-like effects

Three design scenarios were considered to evaluate the impact of adjusting the DCM to NS conditions. All of them refer to a hypothetical 200-km long strike-slip seismic source and two possible construction sites (Figure 2). Site A is aligned with the fault's strike and is located at a distance of 5 km off the tip. Site B is at 9 km from the same extremity, but in a direction normal to the fault's strike.

The main criterion for selecting these specific positions relative to the fault was for the two sites to exhibit the same level of design hazard (i.e., elastic spectrum ordinates) over a period range of interest ($T = 0.50\,s \div 1.00\,s$), when said hazard is estimated by means of *classical* PSHA (i.e., where NS effects are not explicitly considered [23]) for a return period of 975 year. This was to ensure that similar structures located at either of these sites would be designed to resist the same base shear. Thus, observed differences in terms of R will be attributable to NS effects, as will be elaborated later on. In order to also exclude potential soft soil site effects, subsoil conditions at both sites were taken to correspond to stiff soil deposits with a shear wave velocity averaged over the first 30 m of terrain, $V_{s,30}$, equal to 400 m/s.

The first two design scenarios correspond to these two sites when seismicity on the fault is (arbitrarily) assumed to follow a Gutenberg–Richter (G-R) [24] relationship bounded between
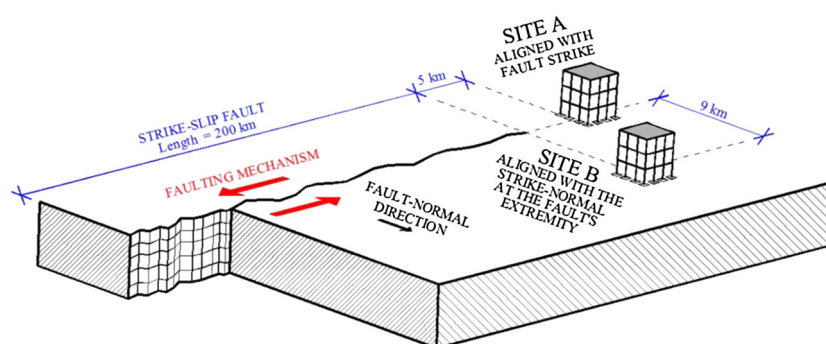
Figure 2. Schematic representation of site-source configuration for the design scenarios considered.

magnitude (M) 4.5 and M 7.5, with unit negative slope and a mean annual rate of event recurrence $v = 0.20$. A third design scenario, the choice of which will be clear later on, was also considered with reference to Site A. In this case, source seismicity was assumed to correspond to a simplified characteristic earthquake (CE) model; that is, a single magnitude M 7.0 is assumed. Annual rate of earthquake recurrence for the third scenario was assumed to be one event/200 years ($v = 0.005$), which was selected on the basis that classical hazard in the $T = 0.50\,s \div 1.00\,s$ range be approximately equal to the one resulting from the G-R model assumption. This extends the premise of shared design spectral values among all considered scenarios.

Recalling the assumption that earthquake recurrence follows a homogeneous Poisson process, uniform hazard spectra (UHS) were computed for two return periods, $T_R = 975$ years and 2475 years, for all three scenarios. The UHS from classical hazard calculations are shown in Figure 3a.

Regarding NS-PSHA, point A and point B were intentionally selected to correspond to site-to-source configurations both prone to FD effects, yet to a different extent; for example, the probability that the 2475 years return period $S_a(T = 0.50s)$ will be exceeded due to an impulsive—rather than an ordinary—record was computed to be 76% for Site A, whereas for Site B, the same probability was found to be 32% (assumptions underlying these calculations to follow). In all three scenarios, seismic hazard was calculated through NS-PSHA (as outlined in Section 4). For this computation, a uniform distribution of potential epicenters along the fault was assumed.

The UHS were computed for the same two return periods of 975 and 2475 years as in the classical hazard case earlier. In Figure 3b, the NS spectra for the three cases are presented. Note that in the G-R scenario, there is visible spectral amplification due to FD—with respect to the classical (Figure 3a) case—mostly
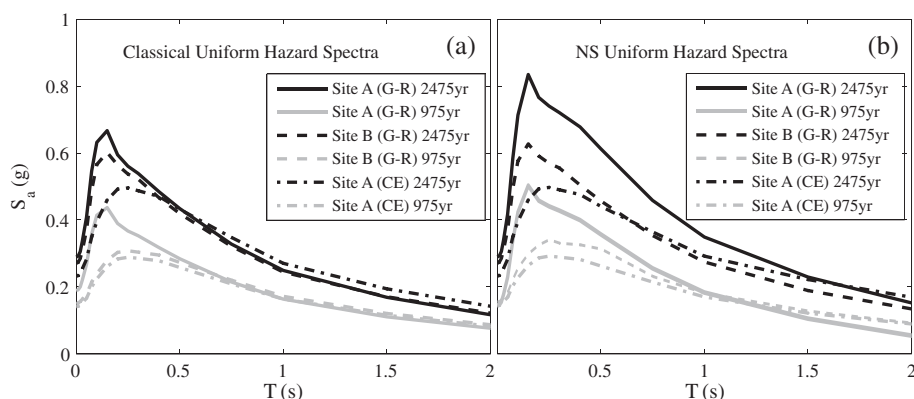
Figure 3. Uniform hazard spectra computed for the various design scenarios by either performing classical probabilistic seismic hazard analysis calculations (a) or by considering near-source forward activity effects in the hazard computation (b).

affecting periods around $T = 0.50\,s$. This is a consequence of T_p dependence on causal magnitude combined with the narrowband amplification scheme [2] adopted in the NS-PSHA calculations (note that the exponential magnitude distribution of G-R seismicity leads to a preponderance of lower magnitudes in the determination of hazard at nearby sites while median T_p for M 5.0 is 0.43 s). On the other hand, FD in the CE case mostly affects a range of longer spectral periods beyond those represented in the figure, which explains the proximity of the classical and NS-UHS (median T_p for M 7.0 being 3.67 s).

In Table II, $S_a(T)$ values defining NS seismic hazard are reported for the three design scenarios described earlier, two return periods corresponding to design performance levels and three spectral periods (T equal to 0.50, 0.75, and 1.00 s), which correspond to the fundamental periods of the structures considered in the following. The lower spectral ordinates encountered at Site B in comparison with Site A are attributable to the different orientation of the two sites with respect to the fault, which, as mentioned, makes the former less prone to FD (i.e., lower conditional pulse occurrence probability) than the latter [25].

5.2. Disaggregation

Disaggregation of NS hazard was performed conditional on *occurrence* of $S_a(T) = s_a$, at the three periods of vibration in Table II, and for both return periods considered. The PDFs of T_p for the 2475 years return period are shown in Figure 4.

5.3. Structural models

The chosen set of structures consists of three reinforced concrete (R/C) plane frames: a four-story, a five-story, and a six-story frame (Figure 5). They were chosen to correspond to the internal frames of perfectly symmetric buildings without in-fills. Furthermore, structure geometry was selected so that all frames would exhibit first-mode dominated dynamic elastic response (first-mode participating mass ratios in excess of 80%), with first-mode periods of natural vibration T_1 equal to 0.50, 0.75, and 1.00 s, respectively, which justify the period range discussed earlier. The consideration of similar structures—bar first-mode period—was a conscious choice, the objective being to evaluate the potentially different effects of FD at various spectral ordinates, while remaining within the DCM applicability domain.

All three structures were designed against gravity loads and seismic actions according to modern codes [26, 27], in a manner that ensures flexure-dominated inelastic response when subjected to increasing lateral forces. More specifically, each frame was designed for inelastic response corresponding to a *behavior factor* ≈ 4.0 under the actions of the 975 years return period site-specific, classical UHS (Figure 3a). Design values of $S_a(T)$ are given in the last column of Table II. These acceleration values are divided by the behavior factor to determine the actions under which the structures are expected to remain elastic. Material qualities assumed for design were C20/25 for concrete and S500/550 for reinforcing steel [26]. A summary of final detailing is given in Figure 5.

All three frames were considered in the context of each of the three design scenarios described earlier, in the direction normal to the fault's strike (Figure 2), leading to 18 cases because of the two return periods. Inelastic displacement demands were estimated using the DCM at two performance

Table II. Spectral acceleration values at periods of interest.

| | $T_R = 2475$ years | | | $T_R = 975$ years | | | $T_R = 975$ years *classical* hazard, equal in all cases |
| | Site A | | Site B | Site A | | Site B | |
	G-R	CE	G-R	G-R	CE	G-R	
$S_a(T = 0.50s)$	0.612 g	0.466 g	0.456 g	0.418 g	0.296 g	0.309 g	0.293 g
$S_a(T = 0.75s)$	0.458 g	0.382 g	0.352 g	0.294 g	0.221 g	0.229 g	0.215 g
$S_a(T = 1.00s)$	0.348 g	0.303 g	0.271 g	0.213 g	0.167 g	0.172 g	0.161 g
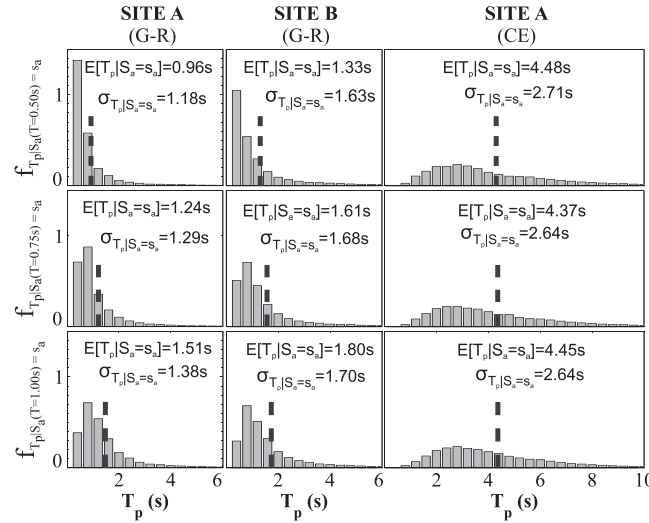
Figure 4. The PDFs of pulse period T_p, resulting from disaggregation of near-source hazard, conditional on pulse occurrence and $S_a(T) = s_a$, referring to 2745 years return period for each scenario (histograms normalized to unit area). Dashed lines indicate the location of the mean, $E[T_p|S_a = s_a]$, whose value is also shown along with standard deviation $\sigma_{T_p|S_a=s_a}$.
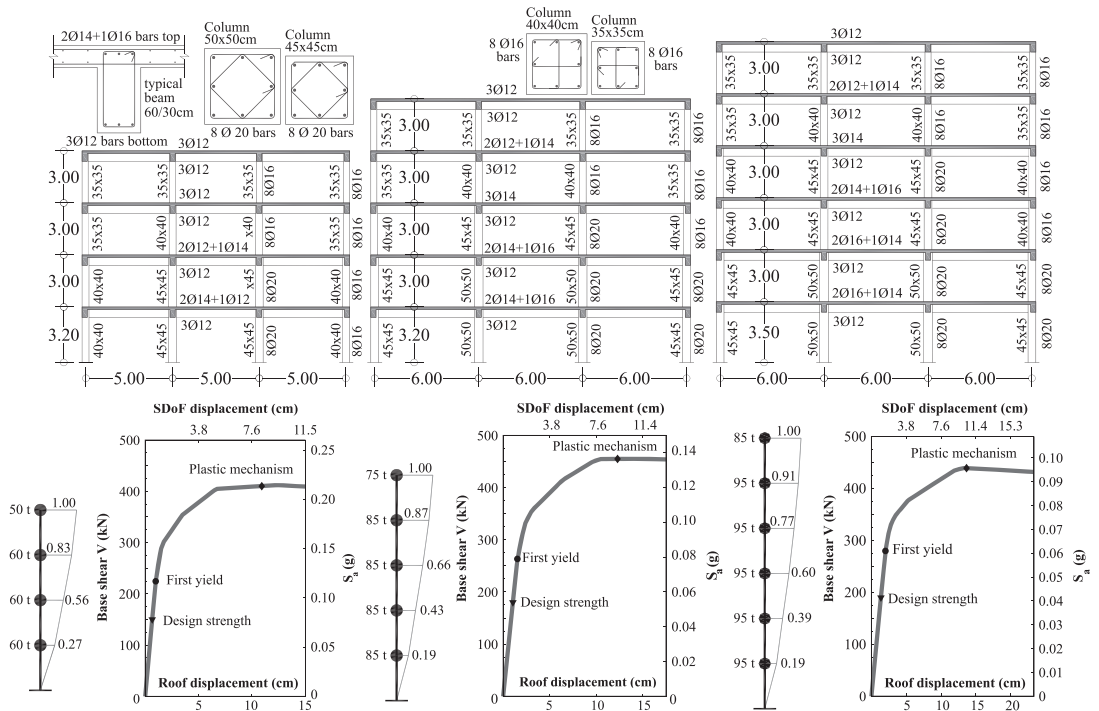
Figure 5. Geometry, detailing (flexural reinforcement), modal information, and pushover curves for the three R/C frames used in the application.

levels: *significant damage*, assumed to correspond to seismic action with a 5% probability of exceedance in 50 years ($T_R = 975$ years), and *near collapse*, corresponding to seismic action with a 2% probability of exceedance in 50 years ($T_R = 2475$ years).

Initially, pushover (base shear versus roof displacement) curves were obtained for all three structures (also shown in Figure 5). The nonlinear structural models built for these inelastic static analyses adopted a lumped plasticity approach, using a multi-linear moment-plastic rotation

relation. The elastic stiffness of R/C members was modeled using a smeared crack approach. Moment-rotation relationships for each member were estimated using mean strength and stiffness properties for confined concrete [28] and reinforcing steel. The bilinear approximations of the resulting relations used the *collapse prevention* limiting values recommended in [12] for ultimate chord rotation capacity.

The static nonlinear (pushover) analyses were carried out by applying a gradually increasing lateral force profile, which remained unchanged throughout each analysis and corresponds to each structure's first-mode excitation to base acceleration (first-mode eigenvectors shown in Figure 5). Second-order (P-Δ) effects were incorporated into the analyses on all accounts, yet collapse mechanisms were characterized by plasticization at the beam ends and the bases of ground floor columns (beam-sway mechanisms), as a consequence of conformity to capacity design rules [27], leading to positive post-yield stiffness of the equivalent SDOF systems.

6. IMPLEMENTING THE DCM IN NS CONDITIONS

Once the pushover curves were obtained, the constituent terms of the right-hand side of Equation (7) had to be estimated separately. For the estimate of the elastic demand, which is needed to compute both $\delta_{t|nopulse}$ and $\delta_{t|pulse}$, the NS-UHS computed for each design scenario and performance level was used (shown in Figure 3b, in addition to which S_a values are given in Table II). Then, the non-impulsive contribution $\delta_{t|nopulse}$ was obtained by simple implementation of the DCM in its traditional form using $C_{R|nopulse}$ from Equation (2), in which subsoil coefficient α was set equal to 90, corresponding to $V_{s,30} = 400$ m/s (NEHRP class C subsoil). For the estimation of the impulsive contribution $\delta_{t|pulse}$, Equations (4) and (6) were used to compute the mean inelastic displacement ratio for FD ground motions, $C_{R|pulse} = E[C_R|S_a(T) = s_a, pulse]$.

It is to recall that these target displacements, in the DCM, are based on a bilinear approximation of the pushover curve, which was constructed via the methodology suggested in [12]. This procedure requires that the bilinear approximation intersect the pushover curve at the target displacement, δ_t, thus resulting in some positive (in this case) post-yield stiffness. This hardening behavior is typically ignored when estimating $C_{R|nopulse}$ via Equation (2). However, this matter will not be discussed here. What should be mentioned is that this method of selecting the equivalent bilinear system, implies that the base shear corresponding to conventional yield, V_y, is dependent on δ_t, thus the evaluation of both the impulsive and non-impulsive contributions requires some iteration for the estimation of strength reduction factor [29].

A graphical representation (corresponding to the converged iteration) for each of the two inelastic displacement contributions considered in Equation (7), is given in Figure 6 for the
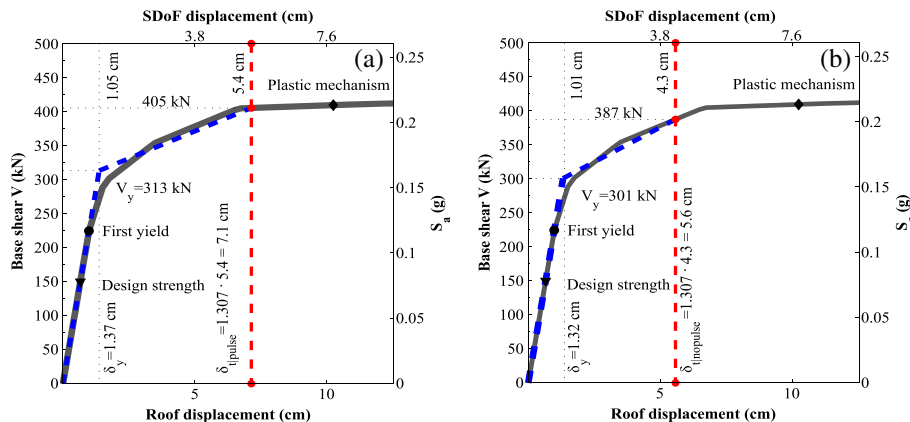
Figure 6. Graphical representation of application of the displacement coefficient method for a four-story R/C frame (T = 0.50 s) at Site A under G-R seismicity. Target displacement estimates for near collapse performance level ($T_R = 2475$ years) considering impulsive (a) and non-impulsive (ordinary) contributions (b).

four-story frame situated at Site A, under the assumption of G-R seismicity and for the near collapse performance level.

Given that, under these conditions, a 74% probability was computed for pulse occurrence conditional to the hazard threshold (i.e., from disaggregation of NS hazard), applying Equation (7), one obtains the result in Equation (8).

$$\delta_t^{NS} = \delta_{t|pulse} \cdot 0.74 + \delta_{t|nopulse} \cdot 0.26 = 7.1 \cdot 0.74 + 5.6 \cdot 0.26 = 6.7 \text{ cm} \tag{8}$$

So as to better appreciate this result, it is useful to also obtain a target displacement without explicitly accounting for FD effects, hereafter termed ordinary target displacement, δ_t^{ord}. In order to evaluate δ_t^{ord}, one simply has to use the classical DCM (Equation (1)) and the classical PSHA uniform hazard spectrum corresponding to each design scenario (Figure 3a) to represent elastic demand. For the case, Equation (8) refers to (four-story frame at Site A, G-R seismicity, near collapse), one obtains $\delta_t^{ord} = 3.8$ cm, which means that accounting for FD lead to a 77% increase in target displacement. It may be worthwhile to underline that both target displacements $\delta_{t|nopulse}$ (ordinary component of NS demand) and δ_t^{ord} (no consideration of NS effects) are derived by applying coefficient $C_{R|nopulse}$ (Equation (2)), valid for ordinary ground motions, yet using different spectral values (from NS-PSHA and classical PSHA, respectively).

The results of the application of the DCM to all cases presented in the previous section are summarized in Table III to facilitate comparisons. It can be observed that the effect of FD on inelastic displacement demand was more pronounced for lower performance levels, which correspond to longer T_R.

A number of observations can also be made, by comparing the DCM estimates of inelastic displacement demand among the design scenarios considered herein. A comparison between Site A and Site B, under the working assumption that seismic hazard at both sites is dictated by the same single source following a G-R law, must necessarily focus on the fact that the position and orientation of Site A relative to the fault, is decidedly more unfavorable than that

Table III. Summary of target displacement estimates resulting from application of the displacement coefficient method. Two different performance levels per design scenario, per structure considered. Column $C_{R|pulse}$ reports mean inelastic displacement ratio conditional on pulse occurrence, whereas $C_{R|nopulse}$ denotes mean inelastic displacement conditional on no pulse occurring.

	T_R	First mode period (s)	$C_{R|pulse}$	$C_{R|nopulse}$	$\delta_{t|pulse}$ (mm)	$\delta_{t|nopulse}$ (mm)	$P[pulse|S_a=s_a]$	δ_t^{NS} (mm)	δ_t^{ord} (mm)	$\frac{\delta_t^{NS}-\delta_t^{ord}}{\delta_t^{ord}}$
Site A G-R seismicity model	2475 years	0.50	1.44	1.12	71	56	0.741	67	38	77%
		0.75	1.31	1.06	111	90	0.673	104	63	65%
		1.00	1.21	1.04	137	118	0.629	130	83	57%
	975 years	0.50	1.17	1.08	40	37	0.687	39	24	63%
		0.75	1.09	1.04	60	56	0.602	58	40	46%
		1.00	1.04	1.02	72	70	0.513	71	53	34%
Site A CE model	2475 years	0.50	3.77	1.07	143	40	0.170	58	39	47%
		0.75	3.10	1.04	218	73	0.166	97	71	37%
		1.00	2.51	1.03	248	101	0.165	125	96	30%
	975 years	0.50	3.13	1.05	75	25	0.100	30	24	25%
		0.75	2.03	1.02	83	42	0.073	45	40	12%
		1.00	1.72	1.01	94	55	0.060	57	53	8%
Site B G-R seismicity model	2475 years	0.50	1.62	1.09	60	40	0.280	46	36	27%
		0.75	1.46	1.05	95	68	0.245	75	61	22%
		1.00	1.28	1.03	113	91	0.243	96	81	19%
	975 years	0.50	1.17	1.05	29	26	0.225	27	24	11%
		0.75	1.12	1.03	47	43	0.181	44	40	9%
		1.00	1.06	1.02	60	57	0.150	57	53	8%

of Site B, when potential FD effects are concerned. Although this was in part expected beforehand (given existing empirical models [4] and recent investigations [25]), it is also confirmed in a most emphatic manner by the results of NS-PSHA and hazard disaggregation; probabilities of pulse occurrence given the hazard threshold computed at Site A are more than twice the ones computed for Site B, and the amplification of spectral ordinates at Site A due to FD is accordingly more pronounced (Table II).

Given the occurrence of hazard levels associated with near collapse performance, both sites appear most likely to be affected by pulse-like ground motions characterized by T_p between 0.50 and 1.00 s, with the modal value for each case corresponding to a ratio of $T/T_p \approx 1$. This effect can be affirmed from the left-skewed probability densities of T_p (Figure 4) and can be attributed to the exponential distribution of magnitude associated with the G-R model. As a result, the realization of T/T_p ratios belonging in the range of high inelastic amplification [5–7] is associated with low probability, conditional on the hazard. Thus, the difference between NS and ordinary structural response, at both sites, is primarily influenced by the elastic component, which is duly amplified by the more frequently occurring, shorter duration pulses.

A comparison, regarding FD effects, between the two different seismicity models considered at Site A, comes in stark contrast with the one directly above. The CE model is associated with events of lower rate, yet greater average magnitude and consequently longer expected pulse duration, which leave the elastic spectral ordinates in the range considered largely unaffected (Figure 3 is particularly eloquent to this effect). Furthermore, the conditional probabilities of pulse occurrence from hazard disaggregation are lower than either of the two G-R cases; loosely speaking, the expected long-period pulses, are less likely to be responsible for reaching the hazard threshold at $T = 0.50\,s \div 1.00\,s$ than ordinary ground motions are. However, because of the fact that the higher mean T_p corresponds to a T/T_p ratio, which translates into potentially aggressive pulse-like ground motions, expected inelastic demand is almost as large as under the G-R model scenario. In other words, the CE seismicity model, presents a case where, *for a given range of periods*, the NS elastic response spectrum hardly departs from the traditional case, and yet expected inelastic demand greatly supersedes that of the classical case, resulting as a weighted average between the more frequent, benign ground motions and some rare pulse-like ground motions, which can cause larger excursions into inelasticity.

7. DCM VERSUS NON-LINEAR DYNAMIC ANALYSIS

Even though validating the results of nonlinear static procedures is an open issue in earthquake engineering (e.g., [30]) and remains beyond the immediate purposes of the work presented herein, which acknowledges the DCM as an established procedure, it may be useful to confirm that dynamic RHA using recorded ground motions, consistent with the models earlier, provide comparable design targets. With this aim, out of the various cases addressed in the preceding sections, two were selected: the five-story and six-story frames ($T_1 = 0.75\,s$ and $1.00\,s$, respectively) subjected to the 975 years return period seismic hazard at site A in the M 7.0 CE scenario.

7.1. Selection of ordinary records

In this exercise, the pulse-like and non-pulse-like cases were treated separately with regard to the selection of real ground motions. For the non-pulse-like case (indicated earlier by the *nopulse* notation), a suite of 20 ordinary records was selected to match a target spectrum using the methodology proposed in [31]. The said target spectrum is a *conditional mean spectrum*, whose computation requires the average causal magnitude and *Joyner-Boore* distance, $\left(\overline{M}, \overline{R}_{JB} \right)$, given absence of a directivity pulse. These values are obtainable from disaggregation of the 975 years NS seismic hazard, at the two considered structural periods and are reported in Table IV, along with the number of standard deviations (in log-space) that separate the design value of $S_a(T)$ from the median conditional to magnitude and distance—a parameter known as epsilon (ε). Having obtained

Table IV. Results from disaggregation of near-source hazard (given absence of directivity pulse and occurrence of S_a) used for the selection of the ordinary ground motion record set.

T_1	$S_a(T_1)$	$\overline{M}$	$\overline{R}_{JB}$	$\varepsilon(S_a)$
0.75 s	0.221 g	7.0	48.5 km	0.865
1.00 s	0.167 g	7.0	52.6 km	0.897

$\left(\overline{M}, \overline{R}_{JB}, \varepsilon\right)$, the conditional mean spectral values at other periods and their conditional variances could be calculated, using the ground motion prediction equation in [32] and the correlation model of [33], for each of the two cases.

As can be seen in Table IV, the values assumed by the conditioning parameters differ only slightly between the two cases, leading to similar shapes of conditional mean spectra. For this reason, a single suite of records was chosen to represent the ordinary component of seismic hazard at both periods (naturally with differing scale factor). The selected records (Table A.I) are from a subset of the NGA database [31] from which pulse-like ground motions were excluded, and each was linearly scaled to exhibit the design $S_a(T)$. This ground motion selection strategy is summarized in terms of response spectra in Figure 7a, where the target conditional mean spectrum can be seen and where each individual record has been scaled at a common $S_a(0.75s) = 0.221$ g.

7.2. Selection of pulse-like records

For the pulse-like case, a different record selection strategy had to be followed, due to the fact that $S_a(T)$ is not a sufficient IM when pulse-like ground motions are concerned [34]. For this reason, some methodologies for the selection and scaling of pulse-like records have been proposed based on advanced IMs [35, 36]; be that as it may, compatibility with current design practice and the DCM requires that reference to the design spectrum—and therefore use of S_a as IM—be maintained.

The problem that the directivity case poses for record selection can be summarized as follows: for a specific structure with given strength, some pulse-like ground motions are particularly *aggressive*, resulting in high ductility demand while others prove relatively *benign*, leading to structural behavior reminiscent of ordinary records. Inclusion of arbitrary numbers of either type of record will thus lead to biased estimates of NS inelastic demand [34]. Ideally,
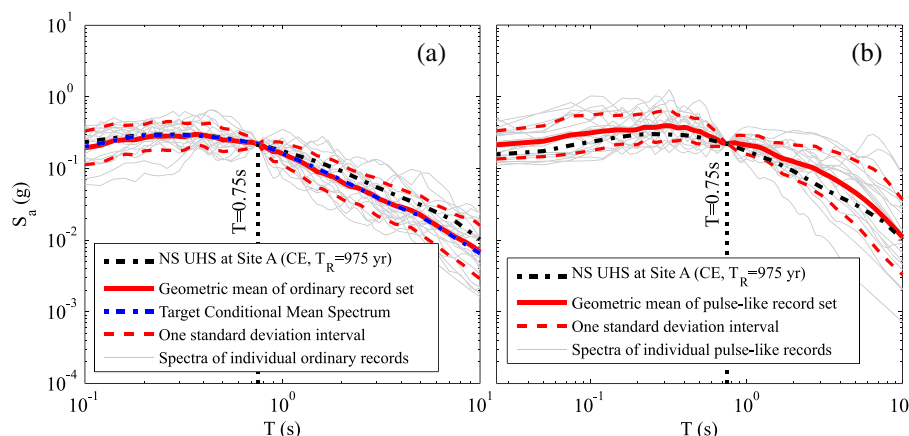
Figure 7. Response spectra of the ordinary (a) and pulse-like (b) scaled records selected for the nonlinear dynamic analysis of the five-story R/C frame (T = 0.75 s). Also shown is the near-source uniform hazard (design) spectrum of the considered scenario and—in the case of the ordinary record set—the target conditional mean spectrum.

assembling a set of pulse-like records that closely reflects hazard at a NS site in terms of pulse period, should address the aforementioned problem, because it is known that T_p plays an important role in determining SDOF and MDOF inelastic demand ([5–7, 18]). However, this is not the case due to the small number of registered directivity ground motions. Indeed, if one attempts to closely match the marginal density of T_p from disaggregation—such as the one presented in Figure 8a—he is faced with the problem that in some T_p intervals, there may be very few records to choose from—if any. Because it is unlikely that a sample as small as a couple of records will reproduce the average trend of inelastic response for some interval of T_p, this can lead to biased estimates of NS inelastic demand. In order to address this problem posed by the relative scarcity of available pulse-like records within some specific T_p range restrictions, the following steps were taken: first, the cumulative distribution function of T_p was used to divide the available dataset of pulse-like ground motions, which consists of the impulsive records used in [6] with the addition of some records from the 1999 Chi-Chi (Taiwan), 2010 Darfield and 2011 Cristchurch (NZ) events, into five bins of equal probability (Figure 8b).

Given a target number of 20 pulse-like ground motions for the selection, this entails extracting four records from each bin. This strategy effectively relaxes the requisite of closely reflecting the distribution of T_p predicted by NS hazard yet—as an offset—provides more densely populated
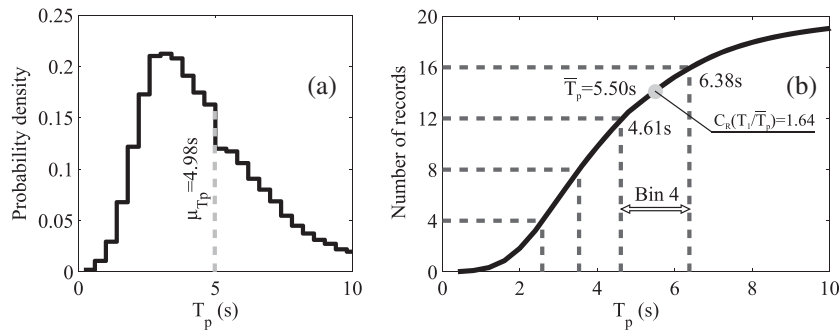
Figure 8. (a) PDF of pulse period from disaggregation of near-source hazard (T = 1.00s, T_R = 975 years) and (b) corresponding cumulative distribution function multiplied by intended number of pulse-like records to be selected and divided into five bins of equal probability for the calculation of inelastic displacement ratio corresponding to the average pulse period of each bin.
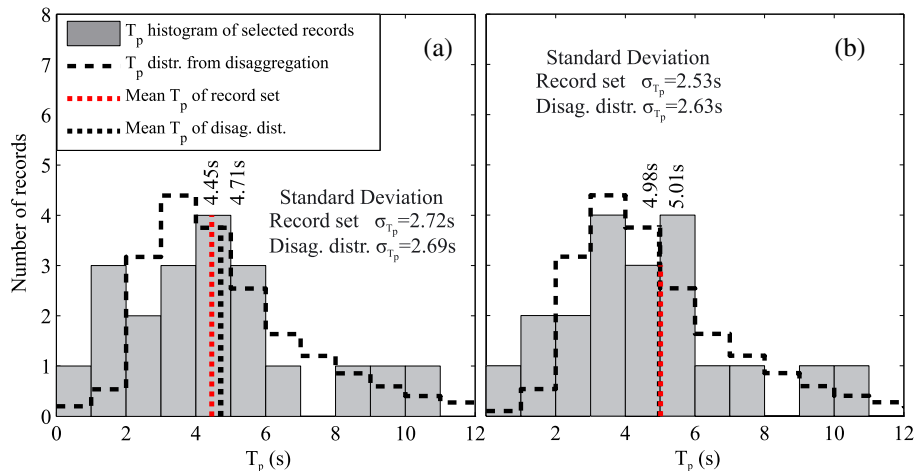
Figure 9. Comparison of target densities of pulse period with T_p histograms of the selected pulse-like ground motion sets for the T = 0.75 s five-story frame (a) and the T = 1.00 s six-story frame (b). The probability densities have been scaled in order for their areas to coincide with those of the histograms. Relevant statistics also are shown.

record bins from which to choose. This procedure is analogous to that employed in [37]. The second step consists in calculating the average pulse period $\overline{T_p}$ for each bin, deriving the corresponding inelastic displacement ratio $C_{R|pulse}(T_1/\overline{T_p})$ from Equation (5) and finally selecting four records from within each bin whose inter-bin average inelastic spectra match this $C_{R|pulse}$ as closely as possible. Thus, even when a bin spans a range of rare pulse periods, such as the one denoted on Figure 8b, the selection is guided toward the average trend exhibited by the entire dataset of impulsive ground motions in an effort to avoid bias due to the scarcity of records within the bin.

This record selection strategy resulted in two sets of pulse-like ground motions being assembled, one for each of the two cases considered. All pulse-like records were scaled to a common spectral ordinate at the first-mode period of each structure. In the case of ordinary ground motions, it has been shown to some extent that this type of scaling does not introduce bias to inelastic response [38]. This approach was maintained for the pulse-like directivity case as well (see, for example, Figure 7b), because the target distributions of T_p were obtained from disaggregation conditional on occurrence of these $S_a(T)$ values. In Figure 9, the degree to which these distributions were matched by the selected record sets can be seen, despite having relaxed this criterion due to the binning strategy adopted. The suites of design ground motions obtained (Table A.II) can be said to reflect the impulsive portion of NS seismic hazard for the considered cases.

7.3. Non-linear response history analyses

Having obtained these record sets, nonlinear models of the two frames were finally each subjected to the two suites of scaled ordinary and pulse-like ground motions. Results in terms of peak roof displacement for each individual record can be found in Tables A.I–II of the appendix. Note that in the case of the six-story frame, the El Centro Array #10 record of the Imperial Valley earthquake (California, 1979) and the Lucerne record of the Landers earthquake (California, 1992) both caused collapse of the structure, even though the level of seismic hazard under consideration corresponds to a damage limitation performance level; thus, the roof displacement values reported in Table A.2 are the maximum values attained prior to the onset of dynamic instability. A summary of the dynamic RHA is given in Figure 10, where relevant response statistics and corresponding DCM estimates, carried over from Table III, are also reported.
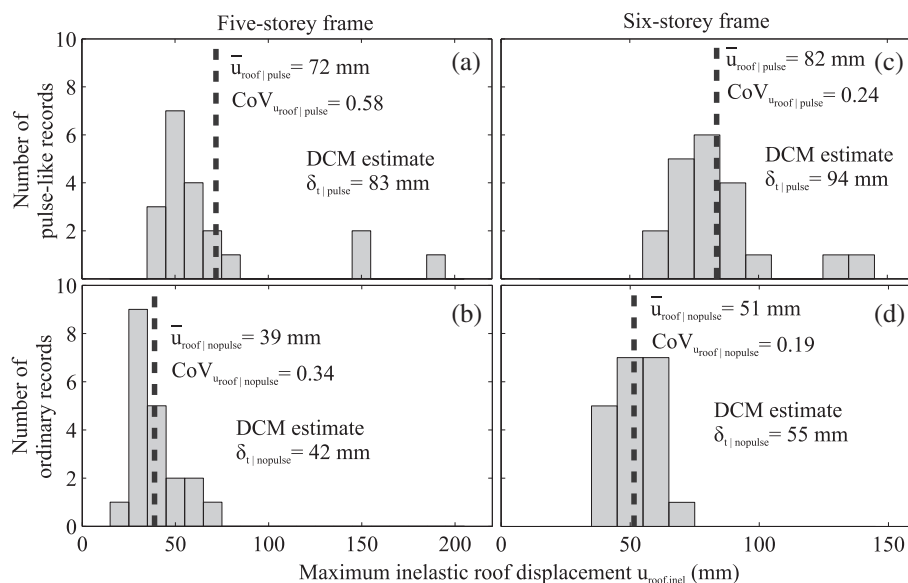
Figure 10. Histograms of maximum inelastic roof displacement resulting from nonlinear dynamic response history analysis for the five-story ($T_1 = 0.75$ s) frame subjected to the pulse-like (a) and ordinary (b) excitation suite as well as the respective results for the six-story ($T_1 = 1.00$ s) frame (c) and (d).

It can be observed that dynamic RHA results indicate an overestimation of inelastic demand due to directivity by the DCM adaptation to NS conditions, of the order of 12%. This can be partly attributed to the fact that the continuous lognormal model of T_p employed during NS-PSHA [19] cannot be effectively reproduced by recorded ground motions due to the rarity of very long duration directivity pulses, in excess of 10 s. Another consideration relevant to the difference between the two estimates, can be the contribution of higher modes to MDOF response; it has been shown in past research that shorter period pulses may excite the higher modes of the structure and particularly influence response at the top stories [18, 35, 39]. However, generally, the RHA confirms the premise that NS inelastic demand due to potential directivity effects can supersede ordinary demand enough to merit special consideration; this, is in agreement with the findings of previous studies [17, 39] (note that [39] dealt with the effect of FD on collapse probability, whereas the present study deals with its effect on mean demand, rather than probability of exceeding capacity).

8. CONCLUSIONS

The presented study dealt with the implementation of the DCM to estimate the design demand for structures in NS conditions. The modifications required to adapt the DCM were discussed both in terms of elastic (i.e., seismic hazard) and inelastic demand. A set of illustrative applications was also provided, where single-fault NS design scenarios, assuming different site-to-source configurations and source seismicity, were considered in order to represent a variety of cases with respect to expected FD effects. The DCM was implemented in this context for modern-code-conforming R/C frames, and compared with design for classical hazard and inelastic demand.

The results may help to quantify the significance of accounting for NS-FD in structural design and assessment. Inasmuch as the DCM can provide a useful estimate of structural seismic performance in the inelastic range, FD was shown to induce appreciable increase—in an engineering sense—in displacement demand. More specifically, increments in the assessment of target displacement due to NS-FD effects range from 34–77% in the case most prone to directivity among those examined, to 8–27% in the case least prone to FD effects among those considered. This behavior was further confirmed when dynamic RHA was performed using suites of ground motions carefully selected in order to reflect NS demand for such a design scenario.

Regarding inelastic structural demand at sites near the source, it was found that this can considerably (percentagewise) exceed demand as computed without accounting for directivity effects, particularly when longer return period performance levels are considered. Furthermore, it was shown that this discrepancy may be exacerbated at sites whose orientation with respect to the fault renders them particularly prone to FD ground motions.

Depending on the distribution of causal event magnitudes most likely to characterize a given source, potential directivity may be manifest by means of relatively short duration pulses, comparable with the periods of natural vibration of typical building structures. This type of impulsive records would mostly affect the elastic response of such structures; that being the case, computing design spectra by means of NS-PSHA should constitute the key step toward estimating NS inelastic response, combined with use of inelastic spectra for NS-FD. However, it was also shown that there are cases where NS effects have small-to-negligible influence on seismic hazard (expressed in elastic response IMs) around a specific spectral region, and yet produce more pronounced increase in mean inelastic demand for structures whose fundamental period places them in that portion of the elastic response spectrum. The nonlinear dynamic analyses carried out corroborate this finding. It was shown that this effect can be explicitly accounted for in structural analysis by use of NS hazard disaggregation results, which provide additional information with respect to the design spectrum.

APPENDIX

Table A.I: Set of ordinary ground motion records used for the RHA of the five-story and six-story frames and results for maximum roof displacement.

No	Earthquake name	Station name	Year	M	Mech.	R_{JB} (km)	ClstD (km)	$V_{s,30}$ (m/s)	PGV (cm/s)	SF T=0.75 s	SF T=1.00 s	$u_{roof,max}$ 5st. (mm)	$u_{roof,max}$ 6st. (mm)
1	Borrego Mountain	San Onofre-So Cal Edison	1968	6.6	S-S	129	129	443	3.7	3.602	3.022	37	49
2	Cape Mendocino	Fortuna-Fortuna Blvd	1992	7.0	R	16	20	457	24.7	0.975	0.907	45	54
3	Chi-Chi, Taiwan	CHY090	1999	7.6	R-O	58	58	215	17.0	1.339	1.154	62	57
4	Chi-Chi, Taiwan	CHY104	1999	7.6	R-O	18	18	223	54.9	0.324	0.544	43	60
5	Chi-Chi, Taiwan	HWA049	1999	7.6	R-O	47	51	273	22.4	0.666	0.710	30	41
6	Chi-Chi, Taiwan	ILA010	1999	7.6	R-O	78	80	474	8.3	1.683	2.812	40	46
7	Chi-Chi, Taiwan	ILA067	1999	7.6	R-O	33	39	553	14.3	0.680	0.643	26	35
8	Chi-Chi, Taiwan	TCU085	1999	7.6	R-O	55	58	1000	7.5	2.787	2.869	32	38
9	Chi-Chi, Taiwan	TTN033	1999	7.6	R-O	56	59	273	6.7	2.323	2.205	73	62
10	Chi-Chi, Taiwan	WNT	1999	7.6	R-O	2	2	664	55.4	0.295	0.317	33	52
11	Chi-Chi, Taiwan-04	CHY035	1999	6.2	S-S	25	25	474	12.3	1.328	0.629	23	48
12	Hector Mine	Little Rock Post Office	1999	7.1	S-S	147	147	442	4.6	1.705	2.361	27	37
13	Hector Mine	Valyermo Forest Fire Station	1999	7.1	S-S	136	136	345	6.2	2.675	3.921	28	60
14	Hector Mine	Wrightwood-Nielson Ranch	1999	7.1	S-S	113	113	345	5.4	2.776	6.346	31	65
15	Kocaeli, Turkey	Tekirdag	1999	7.5	S-S	164	165	660	3.8	2.460	3.161	29	48
16	Landers	Baker Fire Station	1992	7.3	S-S	88	88	271	9.7	1.990	1.522	39	67
17	Landers	La Crescenta-New York	1992	7.3	S-S	148	148	446	3.6	3.557	2.218	62	57
18	Loma Prieta	Bear Valley #10, Webb Res.	1989	6.9	R-O	67	68	304	8.5	1.720	1.850	36	64
19	Northridge-01	West Covina-S Orange Ave	1994	6.7	R	51	52	309	5.8	2.390	1.788	34	43
20	Tabas, Iran	Dayhook	1978	7.4	R	0	14	660	28.2	0.511	0.489	46	47

R_{JB}, Closest distance to horizontal projection of the fault plane.
ClstD, Closest distance to the fault plane.
Rupture mechanisms S-S, strike-slip; R, reverse; R-O, reverse-oblique
PGV, peak ground velocity
SF, scale factor

Table A.II: Set of pulse-like ground motion records used for the response history analysis of the five-story and six-story frames and results for maximum roof displacement.

No	Earthquake name	Station name	Year	M	Mech.	R_{JB} (km)	ClstD (km)	$V_{s,30}$ (m/s)	PGV (cm/s)	T_p (s)	SF T=0.75 s	SF T=1.00 s	$u_{roof,max}$ 5st. (mm)	$u_{roof,max}$ 6st. (mm)
1	Coyote Lake	Coyote Lake Dam (SW Abut)	1979	5.7	S-S	5.3	6.1	597	19.8	0.56	0.809	—	47	—
2	San Fernando	Pacoima Dam (up. left abut)	1971	6.6	R	0.0	1.8	2016	116.5	1.60	0.212	—	62	—
3	Northridge-01	LA Dam	1994	6.7	R	0.0	5.9	629	77.1	1.65	0.225	0.205	55	69
4	Loma Prieta	Gilroy Array #2	1989	6.9	R-O	10.4	11.1	271	45.7	1.72	0.321	0.357	49	67
5	Imperial Valley-06	Agrarias	1979	6.5	S-S	0.0	0.7	275	54.4	2.30	0.533	0.494	41	76
6	Northridge-01	Newhall - W Pico Canyon Rd.	1994	6.7	R	2.1	5.5	286	87.8	2.41	0.290	0.203	81	78
7	Northridge-01	Sylmar - Olive View Med FF	1994	6.7	R	1.7	5.3	441	122.7	3.11	0.277	—	49	—
8	Cape Mendocino	Fortuna - Fortuna Blvd	1992	7.0	R	16.0	20.0	457	22.3	3.14	0.942	—	43	—
9	Imperial Valley-06	EC Meloland Overpass FF	1979	6.5	S-S	0.1	0.1	186	115.0	3.35	0.554	0.315	149	94
10	Northridge-01	Sylmar - Converter Sta	1994	6.7	R	0.0	5.4	251	130.3	3.48	—	0.121	—	62
11	Northridge-01	Sylmar - Converter Sta East	1994	6.7	R	0.0	5.2	371	116.6	3.49	—	0.229	—	61
12	Westmorland	Parachute Test Site	1981	5.9	S-S	16.5	16.7	349	35.8	3.58	0.645	—	58	—
13	Imperial Valley-06	El Centro Array #6	1979	6.5	S-S	0.0	1.4	203	111.9	3.84	—	0.389	—	82
14	Imperial Valley-06	Brawley Airport	1979	6.5	S-S	8.5	10.4	209	36.1	4.03	1.785	0.785	146	78
15	Imperial Valley-06	El Centro Array #5	1979	6.5	S-S	1.8	4.0	206	91.5	4.05	0.404	—	65	—
16	Imperial Valley-06	El Centro Array #10	1979	6.5	S-S	6.2	6.2	203	46.9	4.49	1.576	0.898	195	127*
17	Imperial Valley-06	El Centro Array #4	1979	6.5	S-S	4.9	7.1	209	77.9	4.61	—	0.335	—	73
18	Landers	Lucerne	1992	7.3	S-S	2.2	2.2	685	140.3	5.10	0.327	0.384	49	102*
19	Imperial Valley-06	El Centro Array #3	1979	6.5	S-S	10.8	12.9	163	41.1	5.24	—	1.321	—	89
20	Imperial Valley-06	El Centro Array #8	1979	6.5	S-S	3.9	3.9	206	48.6	5.39	0.551	—	40	—
21	Kocaeli, Turkey	Gebze	1999	7.5	S-S	7.6	10.9	792	52.0	5.87	0.905	0.752	62	79
22	Chi-Chi, Taiwan	TCU101	1999	7.6	R-O	2.0	2.0	273	61.5	6.00	—	0.552	—	91
23	Northridge-01	Lake Hughes #9	1994	6.7	R	24.9	25.4	671	7.3	6.33	4.309	5.287	55	69
24	Imperial Valley-06	El Centro Array #11	1979	6.5	S-S	12.5	12.5	196	41.1	7.36	—	0.783	—	101
25	Darfield, N. Zealand	Templeton School (TPLC)	2010	7.0	R-O	6.0	6.0	250	64.4	8.93	0.920	—	71	—
26	Chi-Chi, Taiwan	TCU128	1999	7.6	R-O	13.0	13.0	600	71.0	9.01	—	0.646	—	92
27	Duzce, Turkey	Lamont 1060	1999	7.1	S-S	25.8	25.9	782	11.3	9.63	6.217	4.191	50	78
28	Chi-Chi, Taiwan	TCU051	1999	7.6	R-O	8.0	8.0	273	41.2	10.39	0.754	—	72	—
29	Chi-Chi, Taiwan	TCU087	1999	7.6	R-O	7.0	7.0	474	41.3	10.40	—	1.093	—	70

*Record caused collapse of the structure; reported roof displacement corresponds to the maximum reliable value from the analysis (maximum roof displacement attained prior to the onset of dynamic instability).

ACKNOWLEDGEMENTS

REFERENCES

1. Somerville PG, Smith NF, Graves RW, Abrahamson NA. Modification of empirical strong ground motion attenuation relations to include the amplitude and duration effects of rupture directivity. *Seismological Research Letters* 1997; **68**:199–222.
2. Baker JW. Identification of near-fault velocity and prediction of resulting response spectra. *Proc Geotech Earthq Eng and Struct Dyn IV*; Sacramento, CA, 2008.
3. Tothong P, Cornell CA, Baker JW. Explicit directivity-pulse inclusion in probabilistic seismic hazard analysis. *Earthquake Spectra* 2007; **23**:867–891.
4. Iervolino I, Cornell CA. Probability of occurrence of velocity pulses in near-source ground motions. *Bulletin of the Seismological Society of America* 2008; **98**(5):2262–2277.
5. Ruiz-García J. Inelastic displacement ratios for seismic assessment of structures subjected to forward-directivity near-fault ground motions. *Journal of Earthquake Engineering* 2011; **15**(3):449–468.
6. Iervolino I., Chioccarelli E, Baltzopoulos G. Inelastic displacement ratio of near-source pulse-like ground motions. *Earthquake Engineering & Structural Dynamics* 2012; **41**:2351–2357.
7. Akkar S, Yazgan U, Gülkan P. Deformation limits for simple non-degrading systems subjected to near-fault ground motions. *Proc 13th World Conf Earthq Eng* 2004; Vancouver BC, Canada, Paper no. 2276.
8. Krawinkler H, Seneviratna GDPK. Pros and cons of a pushover analysis of seismic performance evaluation. *Engineering Structures* 1998; **20**(4-6):452–464.
9. Miranda E, Estimation of inelastic deformation demands of SDOF systems. *Journal of Structural Engineering* 2001; **127**(9):1005–1012.
10. Senevirantna GDPK, Krawinkler HK. Evaluation of inelastic MDOF effects for seismic design. Report no. 120, John A. Blume Earthquake Engineering Center, Stanford University, 1997.
11. BSSC. NEHRP guidelines for the seismic rehabilitation of buildings, FEMA-273, developed by ATC for FEMA, Washington, D.C., 1997.
12. ASCE. Prestandard and commentary for the seismic rehabilitation of buildings, FEMA-356, developed by ASCE for FEMA, Washington, D.C., 2000.
13. FEMA. Improvement of nonlinear static seismic analysis procedures, FEMA-440 prepared by ATC, Washington, D. C., 2005.
14. Chenouda M, Ayoub A. Inelastic displacement ratios of degrading systems. *Journal of Structural Engineering, ASCE* 2008; **134**:1030–1045.
15. Dimakopoulou V, Fragiadakis M, Spyrakos C. Influence of modeling parameters on the response of degrading systems to near-field ground motions. *Engineering Structures* 2013; **53**:10–24.
16. Erduran E, Kunnath SK. Enhanced displacement coefficient method for degrading multi-degree-of-freedom systems. *Earthquake Spectra* 2010; **26**(2):311–326.
17. Akkar S, Metin A. Assessment of improved nonlinear static procedures in FEMA-440. *Journal of Structural Engineering, ASCE* 2007; **133**(9):1237–1246.
18. Alavi B, Krawinkler H. Behavior of moment-resisting frame structures subjected to near-fault ground motions. *Earthquake Engineering & Structural Dynamics* 2004; **33**(6):687–706.
19. Chioccarelli E, Iervolino I. Near-source seismic demand and pulse-like records: A discussion for L'Aquila earthquake. *Earthquake Engineering & Structural Dynamics* 2010; **39**:1039–1062.
20. Chioccarelli E, Iervolino I. Near-source seismic hazard and design scenarios. *Earthquake Engineering & Structural Dynamics* 2013; **42**:603–622.
21. Bazzurro P, Cornell CA. Disaggregation of seismic hazard. *Bulletin of the Seismological Society of America* 1999; **89**:501–520.
22. Benjamin J, Cornell CA. *Probability, Statistics and Decisions for Civil Engineers*. McGraw-Hill: New York, 1970.
23. Reiter L. *Earthquake Hazard Analysis, Issues and Insights*. Columbia University Press: NY, 1990.
24. Gutenberg B, Richter CF. Frequency of earthquakes in california. *Bulletin of the Seismological Society of America* 1944; **34**:185–188.
25. Chioccarelli E, Iervolino I. Sensitivity analysis of directivity effects on PSHA. *Bollettino di Geofisica Teorica ed Applicata* 2014; **55**(1):41–53.
26. CEN. EN 1992-1-1 Design of concrete structures. General rules and rules for buildings, European Committee for Standardization, Brussels, 2004.

27. CEN. EN 1998-1 Design of structures for earthquake resistance – Part 1: General rules seismic actions and rules for buildings, European Committee for Standardization, Brussels, 2004.
28. Mander JB, Priestley MJN, Park R. Theoretical stress-strain model for confined concrete. *Journal of Structural Engineering* 1988; **114**(8):1804–1826.
29. Baltzopoulos G, Chioccarelli E, Iervolino I. Accounting for near-source effects in the displacement coefficient method for seismic structural assessment. *Proc COMPDYN 2013, 4ᵗʰ ECCOMAS Thematic Conf Comp Methods Struct Dyn Earthq Eng*, 2013; Kos Island, Greece, 12–14 June.
30. Kalkan E, Kunnath SK. Assessment of current nonlinear static procedures for seismic evaluation of buildings. *Engineering Structures* 2007; **29**:305–316.
31. Jayaram N, Lin T, Baker JW. A computationally efficient ground motion selection algorithm for matching a target response spectrum mean and variance. *Earthquake Spectra* 2011; **27**(3):797–815.
32. Boore DM, Atkinson GM. Ground-motion prediction equations for the average horizontal component of PGA, PGV and 5%-damped PSA at spectral periods between 0.01 s and 10.0 s. *Earthquake Spectra* 2008; **24**(1):99–138.
33. Baker JW, Jayaram N. Correlation of spectral acceleration values from NGA ground motion models. *Earthquake Spectra* 2008; **24**:299–317.
34. Tothong P, Cornell CA. Structural performance assessment under near-source pulse-like ground motions using advanced ground motion intensity measures. *Earthquake Engineering & Structural Dynamics* 2008; **37**(7):1013–1037.
35. Baker JW, Cornell CA. Vector-valued intensity measures for pulse-like near-fault ground motions. *Engineering Structures* 2008; **30**:1048–1057.
36. Tothong P, Luco N. Probabilistic seismic demand analysis using advanced ground motion intensity measures. *Earthquake Engineering & Structural Dynamics* 2007; **36**:1837–1860.
37. Almufti I, Motamed R, Grant DN, Willford M. Incorporation of velocity pulses in design ground motions for response history analysis using a probabilistic framework. *Earthquake Spectra* 2013; DOI: 10.1193/032113EQS072M (in press).
38. Shome N, Cornell CA, Bazzurro P, Carballo E. Earthquake, records and nonlinear responses. *Earthquake Spectra* 1999; **3**(14):469–500.
39. Champion C, Liel A. The effect of near-fault directivity on building seismic collapse risk. *Earthquake Engineering & Structural Dynamics* 2012; **41**:1391–1409.